



Published in final edited form as:

J Am Chem Soc. 2010 September 15; 132(36): 12690–12697. doi:10.1021/ja104501a.

Autonomous in Vitro Anticancer Drug Release from Mesoporous Silica Nanoparticles by pH-Sensitive Nanovalves

Huan Meng^{†,¶}, Min Xue^{‡,¶}, Tian Xia^{†,¶}, Yan-Li Zhao[#], Fuyuhiko Tamanoi^{§,||}, J. Fraser Stoddart[#], Jeffrey I. Zink^{‡,||,*}, and Andre E. Nel^{†,||,±,*}

[†]Division of NanoMedicine, Department of Medicine, University of California, Los Angeles, California 90095

[‡]Department of Chemistry and Biochemistry, University of California, Los Angeles, California 90095

[§]Department of Microbiology, Immunology, and Molecular Genetics, University of California, Los Angeles, California 90095

^{||}California NanoSystems Institute, University of California, Los Angeles, California 90095

[#]Department of Chemistry, Northwestern University, Evanston, Illinois 60208

[±]The Southern California Particle Center, University of California, Los Angeles, California 90095

Abstract

Mesoporous silica nanoparticles (MSNP) have proven to be an extremely effective solid support for controlled drug delivery on account of the fact that their surfaces can be easily functionalized in order to control the nanopore openings. We have described recently a series of mechanized silica nanoparticles, which, under abiotic conditions, are capable of delivering cargo molecules employing a series of nanovalves. The key question for these systems has now become whether they can be adapted for biological use through controlled nanovalve opening in cells. Herein, we report a novel MSNP delivery system capable of drug delivery based on the function of β -cyclodextrin (β -CD) nanovalves that are responsive to the endosomal acidification conditions in human differentiated myeloid (THP-1) and squamous carcinoma (KB-31) cell lines. Furthermore, we demonstrate how to optimize the surface functionalization of the MSNP so as to provide a platform for the effective and rapid doxorubicin release to the nuclei of KB-31 cells.

Introduction

Mesoporous silica nanoparticles¹ (MSNP) are versatile, noncytotoxic solid supports for nanovalve-controlled drug delivery.² Mechanized silica nanoparticles that are capable of stimuli-responsive release of cargo molecules are presently under active investigation.³ A key challenge for these integrated systems is whether they can be designed for biological use through autonomously controlled nanovalve opening inside cells of interest. Herein, we report a MSNP delivery system based on the operation of supramolecular nanovalves that

© 2010 American Chemical Society

anel@mednet.ucla.edu; zink@chem.ucla.edu.

[¶]These authors contributed equally to this work.

Supporting Information Available: ¹³C-CPMS NMR and ²⁹Si-CPMS NMR spectra, pore surface optimization, cargo release profiles in cell culture medium, apoptosis induced by doxorubicin-loaded MSNP with or without NH₄Cl treatment, and MTS assay of unloaded MSNPs, Figures S1–S5, and physicochemical characterization of cargo-loaded MSNP, Table S1. This material is available free of charge via the Internet at <http://pubs.acs.org>.

are tightly closed at physiological pH (7.4) but capable of opening and delivering drugs in acidifying cellular compartments. We demonstrate how to optimize the system for operation at certain pH levels for the efficient release of some drug molecules by varying the surface functionalization of the nanopores. The operation of this autonomous integrated nanosystem with appropriate design features is demonstrated in human differentiated myeloid (THP-1) and squamous carcinoma (KB-31) cell lines.

The MSNP employed in this work are ~100 nm spheres containing ordered two-dimensional hexagonal arrays of tubular pores with diameters of ~2 nm. The nanopores are large enough to contain common biological dyes and anticancer drugs, yet small enough to be blocked by macrocyclic organic molecules, such as the cyclodextrins. There is currently much interest³ in developing stimuli-responsive methods for controlling access to and from the nanopores. These methods range from coating the nanoparticles with polymers⁴ to controlling individual nanopores with molecules that undergo large-amplitude motions.^{2b} The latter offers the highest degree of control because the “gatekeeper” molecules are bonded covalently inside or at the entrances of the nanopores.^{3a} The MSNP pores also have been functionalized with nanoimpellers, or supramolecules, including pseudorotaxanes, as well as molecules, such as bistable rotaxanes and simpler rotaxanes of the “snap-top” variety^{3a} at the nanopore entrances. These systems respond to physico-chemical stimuli such as light, oxidation/reduction, enzymes, and changes in pH in order to release the trapped cargo molecules.⁵ For in vitro or in vivo biological applications, both external stimuli (such as light^{5a}) as well as autonomous conditions (for example, intracellular enzymes^{5b} or pH^{5c-g}) can be used. In this paper, we demonstrate the autonomous activation of supramolecular nanovalves on mechanized silica nanoparticles initiated by intracellular pH changes without invasive control.

Experimental Section

Materials

3-Aminopropyltriethoxysilane (APTS, 99%), ammonium chloride (>99%), cetyltrimethylammonium bromide (CTAB, 90%), β -cyclodextrin (98%), *N,N'*-dicyclohexylcarbodiimide (99%), doxorubicin (98%), FITC-dextran (MW = 70 000), fluorescein isothiocyanate (FITC, 90%), phorbol-12-myristate-13-acetate (PMA, >99%), 1-pyreneacetic acid (97%), tetraethyl orthosilicate (TEOS, 90%), and 3-(trihydroxysilyl)propyl methylphosphonate monosodium aqueous solution (42%) were purchased from Sigma. *N*-(2-Aminoethyl)-3-aminopropyltrimethoxysilane (90%) and chloromethyltrimethoxysilane (90%) were obtained from Gelest. Benzimidazole (98%) was purchased from Fluka. Apoptosis TUNEL detection kit (Click-iT TUNEL kit), bovine serum albumin (BSA), DPBS solution, L-glutamine, Hoechst 33342, penicillin, RPMI 1640 medium, streptomycin, and wheat germ agglutinin were obtained from Invitrogen. Fetal calf serum (FCS) was purchased from Atlanta Biologicals. Mouse-anti-human mAb (H4A3) was purchased from Abcam. All reagents were used without further purification. Mono(6-diethylenetriamino-6-deoxy)- β -cyclodextrin was prepared according to literature procedures.⁶

Synthesis of MSNP

In a typical synthesis, cetyltrimethylammonium bromide (CTAB, 250 mg, 0.7 mmol) was mixed with NaOH solution (875 μ L, 2 M) and H₂O (120 mL). The mixture reaction was heated to 80 °C. Fluorescein isothiocyanate (2.7 mg) was dissolved in absolute EtOH (1.5 mL) and mixed with 3-aminopropyltriethoxysilane (6 μ L) for 2 h. After the temperature had stabilized, tetraethyl orthosilicate (1.2 mL) was mixed with the ethanolic FITC-APTS solution and added to the CTAB solution. For amine-modified samples, *N*-(2-aminoethyl)-3-aminopropyltrimethoxysilane [60 (5% w/w), 90 (7.5% w/w) or 120 (10% w/w) μ L] was

mixed with TEOS-FITC-APTS solution. For phosphonate-coated nanoparticles, 3-(trihydroxysilyl)propylmethylphosphonate (315 μL) was added to the solution after 15 min. The solution was stirred vigorously at 80 $^{\circ}\text{C}$ for 2 h. The synthesized nanoparticles were centrifuged and washed with MeOH.

Synthesis of 1-Methyl-1*H*-benzimidazole (MBI)-Modified Nanoparticles

Benzimidazole (24 mg, 0.2 mmol) was dissolved in anhydrous *N,N'*-dimethylformamide (DMF, 2.2 mL). Tetrabutylammonium iodide (4 mg) and anhydrous NEt_3 (0.3 mL) were added into the solution, followed by adding chloromethyltrimethoxysilane (30 μL). The solution was heated to 70 $^{\circ}\text{C}$ under N_2 for 24 h. The solvent was then removed in vacuo and the resulting mixture was washed with hexane. The mixture was added to a PhMe/EtOH suspension (40 mL of PhMe and 1 mL of EtOH) of the as-synthesized MSNP (200 mg). The suspension was refluxed under N_2 for 12 h, centrifuged, and washed with MeOH. The CTAB surfactants were removed by dispersing the as-synthesized materials in MeOH (60 mL) and concentrated HCl (2.3 mL, 12 M), and refluxed under N_2 for 12 h. The materials were collected by centrifugation and washed with MeOH.

Synthesis of Pyrene-Modified β -Cyclodextrin

Mono(6-diethylenetriamino-6-deoxy)- β -cyclodextrin (1.22 g, 1.0 mmol) and *N,N*-dicyclohexylcarbodiimide (0.21 g, 1.0 mmol) were dissolved in DMF (30 mL) in the presence of a small amount of 4 \AA molecular sieves under an atmosphere of Ar. 1-Pyreneacetic acid (0.26 g, 1.0 mmol) was dissolved in DMF (10 mL) and then added dropwise into this solution. The reaction mixture was stirred for 2 days in an ice bath and then for another 2 days at room temperature, before being left to stand for 5 h until no more precipitate was deposited. The precipitate was removed by filtration, and the filtrate was poured into acetone (150 mL). The precipitate that formed in acetone was collected by filtration and subsequently purified on a Sephadex G-25 column with water as eluent. After the residue had been dried in vacuo, a pure sample (0.66 g, 45%) of mono[6-(1-pyreneacetamido)diethylenediamino-6-deoxy]- β -cyclodextrin was obtained as a colorless solid. ^1H NMR (500 MHz, D_2O , 25 $^{\circ}\text{C}$, TMS): δ = 2.48–2.61 (m, 8H, $\text{NCH}_2\text{CH}_2\text{N}$), 3.58–3.86 (m, 42H), 4.21 (s, 2H, COCH_2Py), 4.95–5.04 (m, 7H), 7.86–8.11 ppm (m, 9H, Py-H); MS (HR-MALDI): Calcd for $\text{C}_{64}\text{H}_{93}\text{N}_3\text{O}_{35}$ m/z 1463.56, found m/z 1462.56 [M^+].

Drug Loading

For Hoechst 33342 loading, MBI-modified nanoparticles (50 mg) were mixed with Hoechst 33342 (5 mL) in aqueous solution (1 mM). The suspension was stirred for 12 h before β -cyclodextrin (200 mg) or pyrene-modified β -cyclodextrin (200 mg) was added. The mixture was stirred for another 12 h, and the nanoparticles were centrifuged and washed with H_2O .

For doxorubicin loading, MBI-modified nanoparticles (10 mg) were mixed with an aqueous solution (0.25 mL, 4 mg mL^{-1}) of doxorubicin and stirred for 12 h. Then, β -cyclodextrin (40 mg) was added before stirring for another 12 h. The sample was then centrifuged and washed with H_2O .

Assessment of Drug Release

The release profiles were obtained by time-resolved fluorescence spectroscopy, as previously described.^{5d} Briefly, a probe beam (448 nm, 20 mW for doxorubicin-loaded samples; 377 nm, 16 mW for Hoechst-loaded samples; 351 nm, 20 mW for pyrene-modified β -CD) was directed into the water or cell culture medium to excite the dissolved cargo molecules. The luminescence spectrum of the dissolved cargo was collected in 1 s intervals over the course of the experiment. 0.1 M HCl was added to decrease the pH to desired value.

The luminescence intensity at the emission maximum of the dye was plotted as a function of time to generate a release profile.

Physicochemical Characterization of MSNP Coated with Nanovalves

MSNP coated with nanovalves were characterized for sizes, zeta potentials, and shapes, respectively. The shapes and porous structures were characterized using transmission electron microscopy (JEOL JEM 1200-EX, JEOL USA, Inc., Peabody, MA). The nanoparticle sizes and zeta potentials in pure water, BSA water solution (1 mg mL⁻¹), and cell culture media were measured by ZetaSizer Nano (Malvern Instruments Ltd., Worcestershire, UK). All of the measurements were performed with the nanoparticles suspended in filtered water or filtered cell culture media at 40 µg mL⁻¹ nanoparticle concentration.

Cell Culture

THP-1 and KB-31 cells were maintained in 25 or 75 cm² cell culture flasks in which the cells were passaged every 2–4 days. THP-1 cells were cultured in RPMI 1640 medium containing 10% fetal calf serum, penicillin (100 U mL⁻¹), streptomycin (100 µg mL⁻¹), and L-glutamine (2 mM). Differentiation of THP-1 cells was induced by phorbol-12-myristate-13-acetate (PMA, 100 nM) for 3 days before conducting cellular experimentation. KB-31 cells were cultured in DMEM containing 10% FCS, penicillin (100 U mL⁻¹), streptomycin (100 µg mL⁻¹), and L-glutamine (2 mM).

Lysosomal Localization by Immunocytochemistry

Differentiated THP-1 cells and KB-31 cancer cells were grown on chamber slides and were treated by FITC-labeled unloaded nanoparticles (40 µg mL⁻¹) for 6 h, before being fixed, permeabilized, and labeled with a standard immunocytochemistry protocol. LAMP-1 staining was performed by using a 1:500 dilution of mouse-antihuman mAb (H4A3) for 16 h at 4 °C. This procedure was followed by a TRITC-conjugated 1: 500 dilution of goat-antimouse secondary antibody for 1 h at room temperature. Cell membranes were costained with Alexa Fluor 633 conjugated wheat germ agglutinin (WGA, 5 µg mL⁻¹) in PBS for 30 min. Slides were mounted with Hoechst 33342 and visualized under a confocal microscope (Leica Confocal 1P/FCS) in the UCLA/CNSI Advanced Light Microscopy/Spectroscopy Shared Facility.

Use of Confocal Microscopy To Study Cargo Release from Nanovalve-Coated MSNP

To track cargo release in cells, the cells were placed on chamber slides and exposed to the FITC-labeled nanoparticles for the indicated time. The doses of Hoechst- or doxorubicin-loaded MSNP added to THP-1 cells and KB-31 cells were 10 and 50 µg mL⁻¹, respectively. Confocal images were captured at each time point. Since the cargo release is a proton-sensitive process, we used NH₄Cl (20 mM) to neutralize lysosomal pH. To measure intranuclear Dox release quantitatively, Image J software (version 1.37c, NIH) was used to analyze the nuclear fluorescence.

Measurement of Lysosomal pH

A published method⁷ was used to measure lysosomal/endosomal pH. Since FITC-labeled dextran is endocytized and accumulates in lysosomes, lysosomal pH values can be determined by the changes of this compound's fluorescence spectrum under different pHs⁷ (4.0 to 7.0). First, FITC-dextran (MW = 70 kD, 10 µg mL⁻¹) was incubated at various pH values and a fluorescence intensity at 520 nm was measured at excitation wavelengths of 495 and 450 nm, using a microplate reader (Molecular Devices, SpectraMax M5e). A standard curve was constructed by comparing the fluorescence intensity at the two excitation

wavelengths (495/450 nm) against solution pH. To measure the lysosomal pH with or without the lysosomal neutralizer, THP-1 and KB-31 cells were placed into 25 cm² flasks and incubated with 70 kD FITC-dextran (1 mg mL⁻¹) with or without NH₄Cl (20 mM) for 24 h. To thoroughly remove the extracellular FITC-dextran, the cells were washed five times with cold PBS (Invitrogen). 5 × 10⁶ cells were harvested and resuspended into cold DPBS (1 mL). Cellular fluorescence of cells at 520 nm was measured at excitation wavelengths of 495 and 450 nm. The 495/450 ratio was used to obtain the pH value from the calibration curve.

Cytotoxicity of Doxorubicin-Loaded Nanovalve-Coated MSNP in KB-31 Cells

To measure cytotoxicity of doxorubicin-loaded nanoparticles, a MTS cell viability assay was performed. KB-31 cells were plated at 1 × 10⁴ cells per well in a 96-well plate. To confirm that proton-sensitive drug release leads to cell killing, the effect of NH₄Cl was also investigated. The cells were treated with doxorubicin-loaded MSNP (3–250 μg/mL) for 80 h with or without the addition of NH₄Cl (20 mM). Cell viability was calculated from the absorbance readout at 490 nm.

Apoptosis Assay

A TUNEL detection kit was used, according to the manufacturer's instructions, to study the protective effect of NH₄Cl on doxorubicin-induced apoptosis. Briefly, after treatment with doxorubicin-loaded nanoparticles in the presence or absence of NH₄Cl for 60 h, cells were washed, fixed, and permeabilized before TUNEL staining. The number of TUNEL positive cells was assessed in fluorescent microscope (200×). At least three fields were counted by the same investigator to calculate the percentage of TUNEL positive cells.

Statistical Analysis

Data shown are the mean ± SD for duplicate or triplicate measurements in each experiment, which was repeated at least three times. Differences between the mean values were analyzed by the two-sided Student's *t* test or ANOVA and results were considered statistically significant at *p* < 0.05.

Results and Discussion

A nanovalve delivery system was designed to meet a specific criterion; i.e., the nanovalve must be closed tightly at pH 7.4—the pH of blood—but self-open in acidifying endosomal compartments, such as lysosomes. In order to achieve this objective, it is necessary to construct stalks that can be attached covalently to the nanopore openings and, in turn, will bind a capping agent, capable of blocking the nanopore openings reversibly. The interaction, a function of the binding constant, must be pH-dependent and change from a large value at pH 7.4 to a small one in response to mild endosomal acidification conditions that will trigger the release of the cap. After experimentation with a number of pH-responsive nanovalve components, a series of aromatic amines were chosen as the stalk and β-cyclodextrin (β-CD) as the cap. The β-CD ring encircles the stalks (Figure 1a) as a result of noncovalent bonding interactions under neutral pH conditions and effectively blocks the nanopore openings and traps the included cargo molecules. Lowering of the pH leads to protonation of the aromatic amines, followed by β-CD cap release and cargo diffusion from the nanopores.

Two cell lines were chosen for in vitro biological testing: THP-1 because differentiated THP-1 are macrophage-like and ingest particulate matter in a lysosomal compartment; and KB-31 because it is a doxorubicin-responsive cervical cancer cell that can be used to test effective drug delivery by the mechanized MSNP. In order to achieve the attachment and release of the β-CD caps in the lysosomes of these cells, it was necessary to develop a

nanovalve system that responds to the acidification level ($\text{pH} < 6$) that is attainable in the LAMP-1-positive endosomal compartments of THP-1 and KB-31 cells. After a range of aromatic amines that exhibit different $\text{p}K_{\text{a}}$ values (Table 1) were tested, the *N*-methylbenzimidazole (MBI) stalk (Figure 1b) was chosen as the best candidate. Upon protonation, the mechanized MSNP release their β -CD caps without causing any cytotoxicity.

The nanovalves were attached covalently to MSNP, composed of ~ 100 nm primary nanoparticles with uniform pore size ~ 2 nm, as indicated by TEM (Figure 1c). The MBI stalks were synthesized and attached covalently to the MSNP surfaces by means of a postsynthesis protocol (Figure 1a). The attachment was confirmed by ^{13}C -CPMS NMR and ^{29}Si -CPMS NMR spectroscopies (Supporting Information, Figure S1). The asynthesized nanoparticles exhibited a hydrodynamic radius of 900 nm in H_2O as a result of aggregation. Optimal dispersion of the nanoparticles was achieved by sonication in a 1 mg mL^{-1} solution of BSA in H_2O . This procedure is quite effective for nanoparticle (~ 200 nm) dispersal and ultimately yields negatively charged nanoparticles (zeta potential -7 to -9 mV), most likely as a result of the absorption of proteins from the medium (Supporting Information, Table S1). The nanoparticle size remains stable over 24 h in the complete cell culture medium.

In order to verify the functioning of the nanovalve system at appropriate pH conditions, the functionalized MSNP were first of all loaded by soaking in concentrated solutions of Hoechst 33342 dye or the fluorescent chemotherapeutic agent, doxorubicin. The nanoparticles were then capped with β -CD in a concentrated aqueous solution and washed carefully. The release of the trapped fluorescent molecules was tested in H_2O at $\text{pH} 7.0$ and monitored by time-resolved fluorescence spectroscopy. The capped and loaded nanoparticles were placed in the corner of a cuvette and the surrounding liquid was stirred gently. A probe beam was used to illuminate the liquid above the nanoparticles and to excite the fluorescent molecules as they escaped the nanoparticles. The nanovalves remain closed at $\text{pH} 7$ with no cargo leakage as shown in Figure 2, but upon decreasing the pH to 5, the fluorescent guest molecules were released. In order to demonstrate that this process is accompanied by β -CD release, the β -CD caps were labeled with pyrene. These fluorescent caps were monitored by fluorescence spectroscopy so as to be able to follow their release into the supernatant (Figure 2a). The rapid release curve shows that β -CD release precedes the release of the Hoechst dye.

Curiously, the doxorubicin release was slow and incomplete compared to that of the Hoechst dye. This observation raises the possibility that the cationic nature of this chemotherapeutic agent ($\text{p}K_{\text{a}} = 8.2$) causes it to interact electrostatically with the negatively charged $\text{Si}-\text{O}^-$ groups in the MSNP nanopores and thus are held relatively tightly to the nanoparticles. In order to alleviate this problem and obtain more rapid and complete release of doxorubicin, the next step in the design strategy was to modify the MSNP surface to prevent electrostatic interactions (Supporting Information, Figure S2a). Positively charged ammonium groups were attached to the MSNP surface by a cocondensation method.^{3a} Optimization of the release was achieved by testing a series of concentrations of the ammonium groups to find the cationic density at which the increase in electrostatic interactions—limiting the loading capacity of doxorubicin—is outweighed by an optimal rate of release. Figure S2b (Supporting Information) shows the loading yield of MSNP with different surface modifications. The MSNP at an ammonium concentration of 7.5% (w/w) show a moderate doxorubicin loading (1.7%, w/w): they can, however, release doxorubicin rapidly so that the MSNP yield the maximum drug delivery per unit time (Supporting Information, Figure S2c). Thus, functionalization with 7.5% ammonium was used in all subsequent experiments for doxorubicin delivery. Figure 2b shows the improved pH-dependent release profiles of

doxorubicin from the ammonium-modified compared to unmodified MSNP (Figure 2a). The fine-tuning of the MSNP pores to optimize cargo specific drug delivery is another important design feature of our system.

In order to prove that the nanovalve integrated system remains functional under biologically relevant conditions, including the presence of buffered salts and growth supplements, Hoechst and doxorubicin release were tested in THP-1 and KB-31 cell culture media. The respective release profiles in RPMI 1640 (THP-1) and DMEM (KB-31) are similar to those in H₂O, and are shown in Supporting Information, Figure S3a and S3b. The flat baselines and the typical release curves demonstrate that the nanovalve remains operational under culture media conditions.

In order to determine whether the pH-responsive function is maintained intracellularly, it was necessary to demonstrate that MSNP are taken up and capable of localizing in acidifying endosomal compartments. This objective was accomplished by coincubating the FITC-labeled MSNP with THP-1 and KB-31 cells, followed by conducting confocal microscopy in which the late endosomal and lysosomal compartments were stained with TRITC-labeled anti-LAMP-1 antibody. Imaging of both cell types demonstrated >80% colocalization of the green-labeled nanoparticles with the red-labeled lysosomes (Figure 3a). The lysosomal pH values in these cells were determined by measuring the ratios of fluorescence of FITC-dextran at two excitation wavelengths (495/450 nm) and comparing that to a standard pH curve to calculate lysosomal pH.⁷ The pH values in the acidifying endosomal compartments of THP-1 and KB-31 cells decreased (Figure 3b) to 4.6 ± 0.2 and 5.2 ± 0.1 , respectively. Introduction of the lysosomal pH neutralizer,⁸ NH₄Cl, elevated (Figure 3b) these values to $\text{pH } 6.1 \pm 0.4$ and $\text{pH } 6.2 \pm 0.3$ in THP-1 and KB-31 cells, respectively. Thus, NH₄Cl treatment provides a way of confirming the role of the acidifying intracellular microenvironment for cargo release.

In order to verify these operational limits, confocal microscopy was used to follow the kinetics of Hoechst dye and doxorubicin release in THP-1 and KB-31 cells, respectively. Hoechst-loaded, FITC-labeled MSNP are efficiently taken up (Figure 4a) in THP-1 cells. At the earlier times (1 and 3 h), the Hoechst dye is retained in the nanoparticles that localize in the perinuclear regions as fluorescent blue dots, suggesting that the MSNP delivery system does not leak (Figure 4a). However, this visual image changed after 6 h when the Hoechst dye was released to the nuclei of THP-1 (Figure 4a) and KB-31 (not shown). This release was accompanied by the disappearance of the blue dots in the perinuclear region, while the FITC-labeled nanoparticles could still be visualized at this site for up to 36 h. Moreover, NH₄Cl treatment was quite effective at confining the Hoechst dye and FITC-labeled nanoparticles to the perinuclear regions without observable nuclear staining (Figure 4a, right panel). To quantitatively measure Hoechst release to the nucleus, Image J software was used to quantify the nuclear fluorescence intensity (Figure 4b). The results confirmed a statistically significant decrease in dye release to THP-1 nuclei by NH₄Cl treatment. Similar results were observed when the cells were treated by bafilomycin,⁹ another lysosomal pH-neutralizer that inhibits V-ATPases at lysosomal surface¹⁰ (not shown).

While studying doxorubicin release in KB-31, these cells also efficiently took up FITC-MSNP to the perinuclear regions within 3 h, whereupon there was observable drug release (red fluorescence) to the nucleus (Figure 4c). This release was followed by progressive nuclear changes that reflect the pharmacological effect of the drug, including the formation of apoptotic bodies by 60 h and nuclear fragmentation by 80 h. Again, this visual image was dramatically changed by NH₄Cl treatment, a situation which led to most of the drug being retained inside the nanoparticles and little or no evidence of nuclear staining and cell death (Figure 4c, right panel). This visual impression was further confirmed by Image J software

analysis which showed a statistically significant decrease in nuclear doxorubicin staining in the NH_4Cl -treated cells (Figure 4d). A MTS assay was also performed to confirm that NH_4Cl treatment does indeed have the ability to interfere in cytotoxicity (Figure 4e). While the MSNP nanovalve-functionalized MSNP were devoid of cytotoxicity at nanoparticle doses as high as 250 $\mu\text{g}/\text{mL}$, the doxorubicin-loaded nanoparticles resulted in apoptosis that can be confirmed by TUNEL staining¹¹ (Supporting Information, Figure S4). NH_4Cl treatment interfered in the induction of programmed cell death (Figure S4, Supporting Information). Nondrug loaded MSNP, fitted with nanovalves, do not exert detectable cytotoxicity in either KB-31 cells or the 3T3 normal fibroblast cell line (Figure S5, Supporting Information). This observation is in accordance with the low toxicity of the MBI compound used to construct the nanovalve.¹²

Conclusion

In summary, we demonstrate pH-sensitive nanovalve-functionalized MSNP that function as a drug delivery vehicle in cells. The *N*-methylbenzimidazole stalks with the optimized $\text{p}K_a$ endow the nanovalves with the capability of binding the β -CD ring strongly at pH 7.4 and trapping dye and drug molecules in the nanopores. Deprotonation at pH <6, as in acidifying endosomal compartments, causes dissociation of the β -CD caps and release of the cargo molecules. By modifying the interior of the silica surface, the rate of release of the positively charged doxorubicin molecules was increased. Nanoparticles loaded with Hoechst dye and the anticancer drug doxorubicin were efficiently taken up into acidifying endosomal compartments in THP-1 and KB-31 cells. Doxorubicin release from within the LAMP-1 positive endosomal compartments results in apoptotic cell death in KB-31 cells. The fact that drug release and cell killing can be inhibited by lysosomal pH neutralizer supports the hypothesis that the cargo release is caused by lysosomal acidification. The development of pH-sensitive MSNP, functionalized with nanovalves, could improve the efficacy and safety of drug delivery¹³ for chemotherapeutic agents, for example.¹⁴ We are currently conducting animal studies to demonstrate the efficacy and its improved safety profile of this drug delivery system in human tumor-bearing mouse models. To further improve the targeting capability of the drug delivery system based on mechanized MSNP in vivo, additional surface modifications using conjugating ligands, such as transferrin and folic acid, are also being carried out in our laboratories at this time.

Supplementary Material

Refer to Web version on PubMed Central for supplementary material.

Acknowledgments

This study was funded by the US Public Health Service Grants, RO1 CA133697 and RC2 ES018766, and grant 53292 from the Bill & Melinda Gates Foundation through the Grand Challenges Exploration Initiative. This work is also funded by US DOD DTRA 1-08-1-0041 and the National Science Foundation CHE 0809384.

References

1. (a) Kresge CT, Leonowicz ME, Roth WJ, Vartuli JC, Beck JS. *Nature*. 1992; 359:710–712. (b) Cai Q, Luo ZS, Pang WQ, Fan YW, Chen XH, Cui FZ. *Chem. Mater.* 2001; 13:258–263. (c) Lai C-Y, Trewyn BG, Jeftinija DM, Jeftinija K, Xu S, Jeftinija S, Lin VSY. *J. Am. Chem. Soc.* 2003; 125:4451–4459. [PubMed: 12683815]
2. (a) Vallet-Regí M, Francisco B, Daniel A. *Angew. Chem., Int. Ed.* 2007; 46:7548–7558. (b) Angelos S, Johansson E, Stoddart JF, Zink JI. *Adv. Funct. Mater.* 2007; 17:2261–2271. (c) Xia T, Kovochich M, Liang M, Meng H, Kabehie S, George S, Zink JI, Nel AE. *ACS Nano*. 2009; 3:3273–3286. [PubMed: 19739605]

3. (a) Coti KK, Belowich ME, Liong M, Ambrogio MW, Lau YA, Khatib HA, Zink JI, Khashab NM, Stoddart JF. *Nanoscale*. 2009; 1:16–39. [PubMed: 20644858] (b) Trewyn BG, Slowing II, Giri S, Chen HT, Lin VSY. *Acc. Chem. Res.* 2007; 40:846–853. [PubMed: 17645305] (c) Slowing II, Trewyn BG, Giri S, Lin VS-Y. *Adv. Funct. Mater.* 2007; 17:1225–1236. (d) Slowing I, Vivero-Escoto J, Wu C-W, Lin V. *Adv. Drug Delivery Rev.* 2008; 60:1278–1288.
4. (a) Zhu YF, Shi JL, Shen WH, Dong XP, Feng JW, Ruan ML, Li YS. *Angew. Chem., Int. Ed.* 2005; 44:5083–5087. (b) Zhu C-L, Song X-Y, Zhou W-H, Yang H-H, Wen Y-H, Wang X-R. *J. Mater. Chem.* 2009; 19:7765–7770. (c) Andrew MacKay J, Chen M, McDaniel JR, Liu W, Simnick AJ, Chilkoti A. *Nat. Mater.* 2009; 8:993–999. [PubMed: 19898461]
5. (a) Lu J, Choi E, Tamanoi F, Zink JI. *Small*. 2008; 4:421–426. [PubMed: 18383576] (b) Patel K, Angelos S, Dichtel WR, Coskun A, Yang YW, Zink JI, Stoddart JF. *J. Am. Chem. Soc.* 2008; 130:2382–2383. [PubMed: 18232687] (c) Nguyen TD, Leung KCF, Liong M, Pentecost CD, Stoddart JF, Zink JI. *Org. Lett.* 2006; 8:3363–3366. [PubMed: 16836406] (d) Angelos S, Yang YW, Patel K, Stoddart JF, Zink JI. *Angew. Chem., Int. Ed.* 2008; 47:2222–2226. (e) Du L, Liao S, Khatib HA, Stoddart JF, Zink JI. *J. Am. Chem. Soc.* 2009; 131:15136–15142. [PubMed: 19799420] (f) Angelos S, Khashab NM, Yang YW, Trabolsi A, Khatib HA, Stoddart JF, Zink JI. *J. Am. Chem. Soc.* 2009; 131:12912–12914. [PubMed: 19705840] (g) Liu R, Zhang Y, Zhao X, Agarwal A, Mueller LJ, Feng P. *J. Am. Chem. Soc.* 2010; 132:1500–1501. [PubMed: 20085351]
6. May BL, Kean SD, Easton CJ, Lincoln SF. *J. Chem. Soc., Perkin Trans.* 1997; 1:3157–3160.
7. (a) Ohkuma S, Poole B. *Proc. Natl. Acad. Sci. U.S.A.* 1978; 75:3327–3331. [PubMed: 28524] (b) Cardelli JA, Richardson J, Miers D. *J. Biol. Chem.* 1989; 264:3454–3463. [PubMed: 2492537]
8. (a) Ling H, Vamvakas S, Gekle M, Schaefer L, Teschner M, Schaefer RM, Heidland A. *J. Am. Soc. Nephrol.* 1996; 7:73–80. [PubMed: 8808112] (b) Ling H, Ardjomand P, Samvakas S, Simm A, Busch GL, Lang F, Sebekova K, Heidland A. *Kidney Int.* 1998; 53:1706–1712. [PubMed: 9607203]
9. (a) Masaru H, Shotaro S, Masao Y, Motoaki K, Masahito O, Satoshi S, Yoshihiro M, Kazunori N, Michio S, Kyuichi T. *J. Hepatol.* 1996; 24:594–603. [PubMed: 8773916] (b) Yoshimori T, Yamamoto A, Moriyama Y, Futai M, Tashiro Y. *J. Biol. Chem.* 1991; 266:17707–17712. [PubMed: 1832676]
10. Gagliardi S, Gatti PA, Belfiore P, Zocchetti A, Clarke GD, Farina C. *J. Med. Chem.* 1998; 41:1883–1893. [PubMed: 9599238]
11. Gavrieli Y, Sherman Y, Ben-Sasson SA. *J. Cell Biol.* 1992; 119:493–501. [PubMed: 1400587]
12. Database of Chemical Safety Information from Intergovernmental Organizations. <http://www.inchem.org/documents/jmpr/jmpmono/v073pr11.htm>
13. (a) Leroux J-C, Cozens RM, Roesel JL, Galli B, Doelker E, Gurny R. *Pharm. Res.* 1996; 13:485–487. [PubMed: 8692747] (b) Dai J, Nagai T, Wang X, Zhang T, Meng M, Zhang Q. *Int. J. Pharm.* 2004; 280:229–240. [PubMed: 15265562] (c) Bae Y, Jang W-D, Nishiyama N, Fukushima S, Kataoka K. *Mol. Biosyst.* 2005; 1:242–250. [PubMed: 16880988]
14. (a) Dianxiang L, Xiantao W, Jie L, Zhongwei G, Xingdong Z, Yujiang F. *J. Biomed. Mater. Res., Part B: Appl. Biomater.* 2009; 89B:177–183. (b) Yang Y-J, Tao X, Hou Q, Ma Y, Chen X-L, Chen J-F. *Acta Biomater.* 2010; 6:3092–3100. [PubMed: 20197128] (c) Bae Y, Nishiyama N, Kataoka K. *Bioconjugate Chem.* 2007; 18:1131–1139. (d) Lee ES, Gao Z, Kim D, Park K, Kwon IC, Bae YH. *J. Controlled Release.* 2008; 129:228–236.
15. The average hydroxyl coverage for silica nanoparticles and gels equals 4.9 OH/ nm² Zhuravlev, L. T. *Langmuir* **1987**, 3, 316–318. This value corresponds closely to the value expected if, on average, the amorphous silica surface is represented by the {111} face of cristobalite (Brinker, C. J.; Scherer, G. W. *Sol-Gel Science*; Elsevier Science: New York, 1990; p 624). Based on this model, the distance between two surface OH groups is 5.3 Å. Thus, the number of surface OH groups around one nanopore (nanopore diameter 2.2 nm) is 13. Since the attachment of one stalk on the nanopore requires at least 2 OH groups on the nanopore perimeter, the maximum number of stalks that can become attached to one nanopore is about 6. For a fully assembled nanovalve, the size depends on the β-cyclodextrin—the periphery diameter of the secondary side is ~1.5 nm: Szejtli, J. *Chem. Rev.* **1998**, 98, 1743–1754. Thus, the maximum number of nanovalves per nanopore opening is about 4.

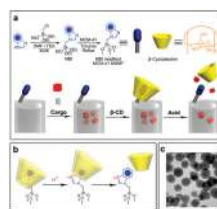


Figure 1.

A graphical representation of the pH responsive MSNP nanovalve. (a) Synthesis of the stalk, loading of the cargo, capping of the pore, and release of the cap under acidic conditions. Based on our calculations,¹⁵ the maximum number of stalks per nanopore is 6, and the maximum number of fully assembled nanovalves per nanopore is 4. The average nanopore diameter of the MSNP is around 2.2 nm, and the periphery diameter of the secondary side of β -cyclodextrin is ~ 1.5 nm. Thus, for a cargo with diameter >0.7 nm, a single nanovalve should be adequate to achieve effective pH-modulated release. (b) Details of the protonation of the stalk and release of the β -cyclodextrin. (c) TEM image of capped MSNP. The scale bar is 100 nm.

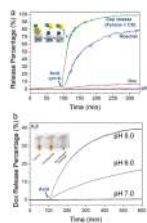


Figure 2. Release profiles of cargo molecules and the cyclodextrin. (a) Fluorescence intensity plots for the release of Hoechst dye, doxorubicin, and the pyrene-labeled cyclodextrin cap released from MSNP. (b) Release profiles of doxorubicin from ammonium-modified (7.5%, w/w) nanoparticles showing the faster and larger response compared to the unmodified MSNP (Figure 2a).

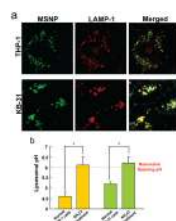


Figure 3.

Cellular uptake and lysosomal pH measurements in THP-1 and KB-31 cells. (a) Confocal microscopy images showing FITC-labeled MSNP uptake into the LAMP-1⁺ compartment in THP-1 and KB-31 cells. The yellow spots in the merged image show the colocalization of the nanovalve MSNP with LAMP-1 positive compartment. The colocalization ratio, as determined by Imaging J software, indicates >80% colocalization of the green-labeled nanoparticles with the red-labeled lysosomes. (b) Measurement of lysosomal pH in THP-1 and KB-31 cells prior to and after NH₄Cl treatment (**p* < 0.05). The dashed line indicates that a threshold pH (6.0) is required for nanovalve opening. Since NH₄Cl treatment elevates the pH to above this threshold, it eliminates the microenvironment that is required for cargo release.

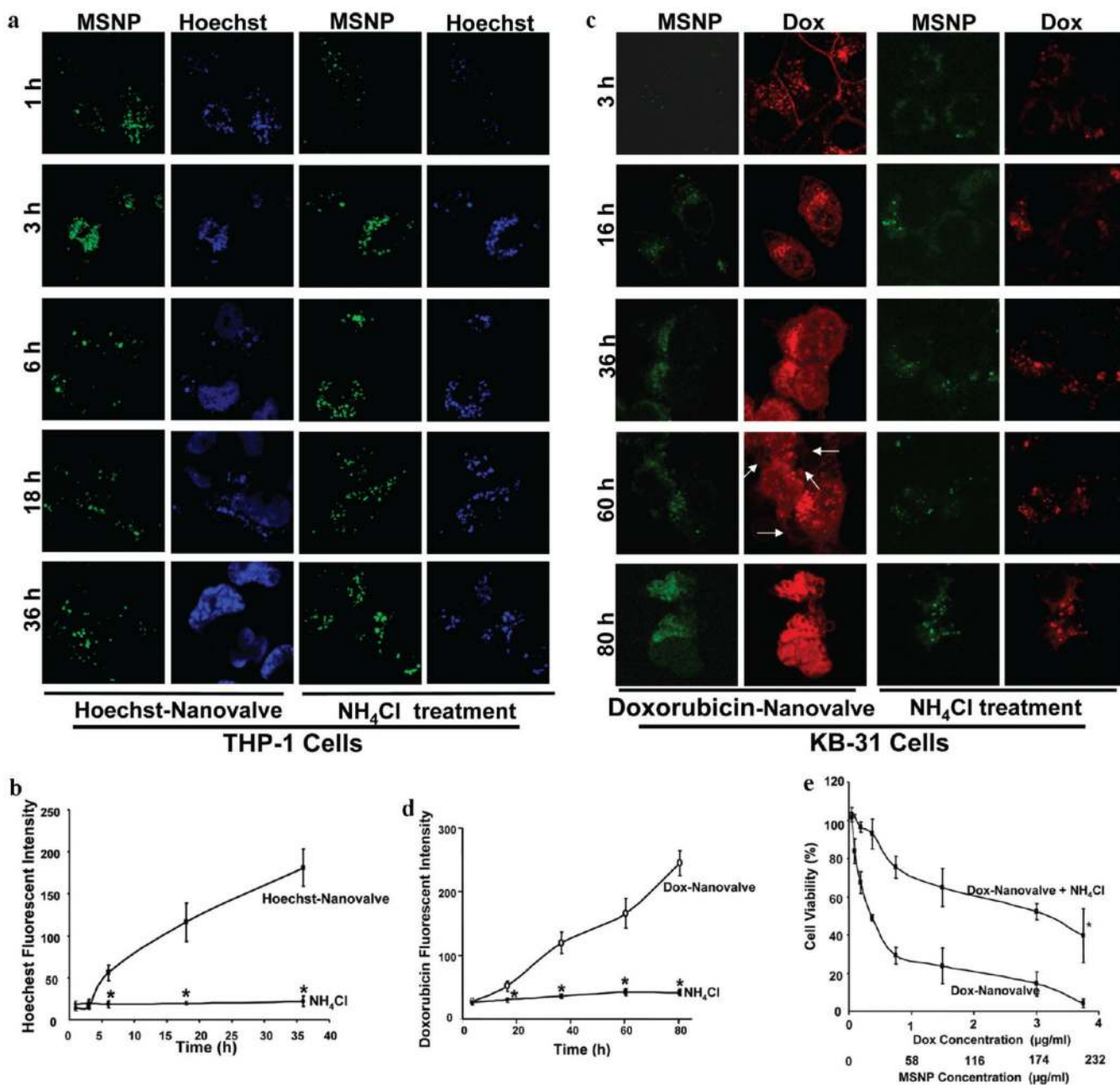
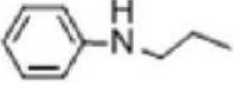
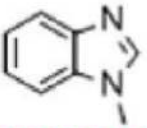
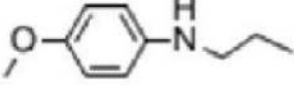
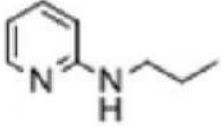
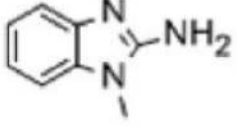


Figure 4. Confocal images of THP-1 and KB-31 cells incubated with MSNP containing Hoechst dye and doxorubicin drug for the indicated times. (a) Hoechst-loaded, FITC-labeled MSNP are efficiently taken up in THP-1 cells. In early time points (1 and 3 h), Hoechst was retained in nanoparticles localized in the perinuclear region. The gradual disappearance of blue dots in perinuclear region and gradual increase in nuclear staining indicate the release of Hoechst dye from the nanoparticle to the nucleus. By 36 h, most of dye was released. NH₄Cl effectively prevented Hoechst release. (b) Quantitative analysis of the nuclear Hoechst fluorescence signal was determined by Image J software in cells with or without NH₄Cl treatment. (c) KB-31 cancer cells effectively endocytosed the doxorubicin-loaded FITC-MSNP at 3 h. This action is followed by doxorubicin release to the nucleus, induction of

cytotoxicity and appearance of apoptotic bodies by 60 h (arrow in Figure 4c), followed by nuclear fragmentation after 80 h. However, with NH_4Cl treatment, most of the doxorubicin was confined to the nanoparticles and hence there was no observable cell death. (d) Quantitative analysis of the nuclear doxorubicin fluorescence signal was determined by Image J software with or without NH_4Cl treatment. (e) Doxorubicin-loaded MSNPs, fitted with a pH nanovalves, inhibited KB-31 viability efficiently as determined by a MTS assay. Doxorubicin-induced cytotoxicity was partially inhibited by NH_4Cl treatment.

Table 1

Optimization of the Operational pH Conditions of MSNP Fitted with Different Stalks To Define Physiologically Responsive Nanovalves^a

Stalk	^a pK _a	Releasing pH	Cap
	5.04	< 5.0	α-CD
	^b 5.67	< 6.0	β-CD
	5.89	< 6.0	α-CD
	6.41	< 7.0	α-CD
	7.66	< 8.0	β-CD

^a(a) The pK_a values were calculated by Advanced Chemistry Development (ACD/Labs) Software V8.14 for Solaris (©1994–2010 ACD/Labs). (b) The pK_a of MBI-β-CD is highlighted in red and represents the stalk chosen for the reported experiments. The release pH increases as the pK_a value of the aromatic group chosen for the stalk goes up. Biocompatible MBI was chosen because the nanovalves are closed tightly in neutral condition but self-open in acidifying endosomal compartments.